Chemistry Europe
European Chemical Societies Publishing

WILEY VCH

Excellence in Chemistry Research



Announcing our new flagship journal

- Gold Open Access
- Publishing charges waived
- Preprints welcome
- Edited by active scientists

Meet the Editors of *ChemistryEurope*



Luisa De Cola
Università degli Studi di Milano Statale, Italy



Ive Hermans
University of Wisconsin-Madison, USA



Ken Tanaka
Tokyo Institute of Technology, Japan

Check for updates

ChemCatChem

Research Article
doi.org/10.1002/cctc.202300687

Chemistry Europe
European Chemical Societies Publishing

www.chemcatchem.org

Special Collection

Elucidating the Effect of Nitrogen Occupancy on the Hydrogen Evolution Reaction for a Series of Titanium Oxynitride Electrocatalysts

Guangmeimei Yang,[a] Yuxiang Zhou,[b, c] Mengnan Wang,[c, d] James Murawski,[c] Louise I. Oldham,[a] Tian Tian,[e] Ifan E. L. Stephens,*[c] and Andreas Kafizas.*[a, b]

Titanium nitride (TiN) shows desirable properties for use as an electrocatalyst and catalyst support, as it possesses high electrical conductivity and excellent corrosion resistance. However, the effect of oxygen content in the nitride lattice on its ability to drive the hydrogen evolution reaction (HER) is not well understood. Here, a series of titanium oxynitrides (TiN_xO_{1-x}) with varied nitrogen occupancy ($0.53 \leq x \leq 1.0$) in the bulk have been fabricated by ammonolysis. Their specific activities towards the HER were normalised by the surface areas determined by BET and electrochemical methods. We show that the specific activities of these oxynitrides are strongly correlated with the bulk nitrogen occupancy, despite the similar surface composition derived from XPS analysis. Furthermore, a removal of the oxygen content in the bulk or at the surface was attributed to the upgraded performance (up to 25% increase) seen during extended chronoamperometry (CA) tests. Our results show that minimising bulk oxygen content in this class of material is critical to achieve a more conductive and active material for the HER.

Introduction

Population growth, coupled with modern society's high dependence on fossil fuels has resulted in a continuous increase of CO_2 concentrations in the atmosphere, which is the primary cause of climate change.[1,2] To curtail CO_2 emissions, and our dependence on fossil fuels, energy generation from renewables is increasing, and when coupled to proton exchange membrane (PEM) electrolysis, can produce clean hydrogen fuel with almost a net-zero carbon footprint.[3] However, commercial PEM electrolysers contain scarce and high-cost platinum group metal catalysts, which may hinder the mass implementation of PEM electrolysers to achieve the terawatt-scale needed to meet global energy demands.[4]

Early transition metal nitrides (ETMNs) have been considered as the alternative to noble metals owing to the low cost, robustness and high conductivity.[5,6] One increasingly popular strategy being explored is to use robust and conductive materials as supports for electrochemical water splitting reactions,[7] where it has been shown that TiN nanoparticles have shown a lower rate of electrochemical oxidation compared with conventional carbon black when supporting platinum under PEM fuel cell conditions.[8] Due to its unique electronic structure and conductivity, TiN was able to bridge oxygen defected TiO_{2-x} and carbon nitride within a heterojunction system for the photocatalytic generation of hydrogen.[9] The high conductivity of TiN comes from the closed-packed structure and excess d-band electrons of the metal atoms.[10,11] The electrical resistivity of the nitride (TiN) has been shown to be ~1.5×10^{-10} Ohm·cm,[12] whereas the electrical resistivity of the oxide (rutile TiO_2) is about 12 orders of magnitude higher (~7.2×10^{2} Ohm·cm).[13]

It is known that transition metal oxides are typically semiconductors or insulators,[14] whereas transition metal nitrides always show high conductivity.[15] For example, TiO_2 has been widely applied in the field of photocatalysis owing to its high activity for a range of reactions and stability but is limited

[a] G. Yang, L. I. Oldham, Dr. A. Kafizas.
Department of Chemistry
Molecular Science Research Hub
Imperial College London
White City, London, W12 0BZ (UK)
E-mail: a.kafizas@imperial.ac.uk

[b] Y. Zhou, Dr. A. Kafizas.
London Centre for Nanotechnology
Imperial College London
London, SW7 2AZ (UK)

[c] Y. Zhou, M. Wang, Dr. J. Murawski, Prof. I. E. L. Stephens
Department of Materials
Imperial College London
London, SW7 2AZ (UK)
E-mail: i.stephens@imperial.ac.uk

[d] M. Wang
Department of Chemical Engineering
Imperial College London
London, SW7 2AZ (UK)

[e] Dr. T. Tian
Barrer Centre
Department of Chemical Engineering
Imperial College London
London, SW7 2AZ (UK)

Supporting information for this article is available on the WWW under https://doi.org/10.1002/cctc.202300687

This publication is part of a Special Collection on "Holistic Development of Electrochemical Processes for Industrial Systems"

© 2023 The Authors. ChemCatChem published by Wiley-VCH GmbH. This is an open access article under the terms of the Creative Commons Attribution License, which permits use, distribution and reproduction in any medium, provided the original work is properly cited.

© 2023 The Authors. ChemCatChem published by Wiley-VCH GmbH

by its wide optical band gap in the UV region for solar applications.[16] Substitutional doping of oxygen with nitrogen atoms in this oxide system is the most popular method for narrowing the band gap of this material.[17] The introduction of nitrogen atoms results in a decrease in energy of the valence band due to the mixing of N 2p orbitals with O 2p orbitals in the density of states.[18] The complete replacement of oxygen with nitrogen results in the formation of a metallic material, titanium nitride (TiN), of rock-salt crystal structure, which has numerous advantageous properties such as ultra-hardness, high electrical and thermal conductivity, but to date, has shown relatively low catalytic performance due to its inert nature and insufficient access to d band electrons.[19] Studies have been carried out to make TiN a better electrocatalyst or catalyst support by increasing its surface area, for example, making TiN nanowires[20,21] and nanotubes.[22] These methods helped achieve better overall activities but made the intrinsic activities per active site mysterious on the other hand. Despite the high bulk stability of TiN, the surface is susceptible to oxidation. Nitrogen defects in the lattice of transition metal nitrides are often filled with oxygen, resulting in the formation of an oxynitride (TiON).[23] Interestingly, recent studies have shown that the activities and selectivity of nitrides towards some electrochemical reactions, oxygen evolution reaction (OER) and oxygen reduction reaction (ORR), are controlled by the degree of oxygen incorporation.[24,25] However, the effect of nitrogen occupancy in TiON regarding the intrinsic activity and conductivity for applications as electrocatalyst or catalyst support in the HER is not currently well understood. To address this, herein, we synthesised a range of titanium oxynitrides (TiN_xO_{1-x}) with varied bulk nitrogen occupancy ($0.53 \leq x \leq 1.0$) and studied their performance towards the electrochemical HER using a rotating disc electrode (RDE). The relationship between the specific activities for the HER of titanium oxynitrides and the nitrogen occupancies within their bulk structures is found to be strongly correlated.

Results and Discussion

The titanium nitride phase is reported to form above 900 °C.[26] Thus, the nitridation temperatures chosen in this work started from 900 °C, and we investigated 1000 °C, 1100 °C and 1200 °C also. These samples were denoted as TiN-900, TiN-1000, TiN-1100, TiN-1200, respectively, with the number indicating the annealing temperature. A commercial TiN powder was purchased and used as a reference, which was denoted as TiN-commercial. XRD patterns of the as-synthesised oxynitride powders confirmed the formation of single-phase rock-salt TiN_xO_{1-x} structures (Figure 1). Early transition metal nitrides with a low oxygen content (< 50 %) will maintain its most stable crystal structure, namely the cubic rock-salt structure.[25] The stoichiometry of the oxynitride TiN_xO_{1-x} controls the phase that forms, with a transmission point of x located between 0.40–0.45.[27] When x is larger than 0.45, the oxynitride adopts the NaCl type structure, i.e., the nitride structure. When x is smaller than 0.4, it will adopt an α-TiO arrangement. Changes in the value of x, within an adopted crystal structure, will cause the peaks in XRD patterns to systematically shift in accordance with Vegard's law (Equation S1).[28] The value of x can be determined if the lattice parameters of the unit cell are calculated and compared with the parent materials; TiO and TiN. The lattice parameters of each oxynitride sample were determined by fitting a Le Bail model to each XRD (Figure S2). Using Vegard's law, each value of x was determined,[28] with x ranging herein from 0.53 to 1.0. All values of x were higher than the transmission point (Table S1), which was supported by the fact that solely the rock-salt structures was observed (Figure 1). Moreover, the derived values of x (nitrogen occupancy) increased almost linearly with annealing temperature.

Even though TiN is thermodynamically stable, oxide layer formation at the surface is still thermodynamically favourable.[29] From XPS analysis, which probes up to ~10 nm deep,[30] the oxynitrides formed at various temperatures show a similar

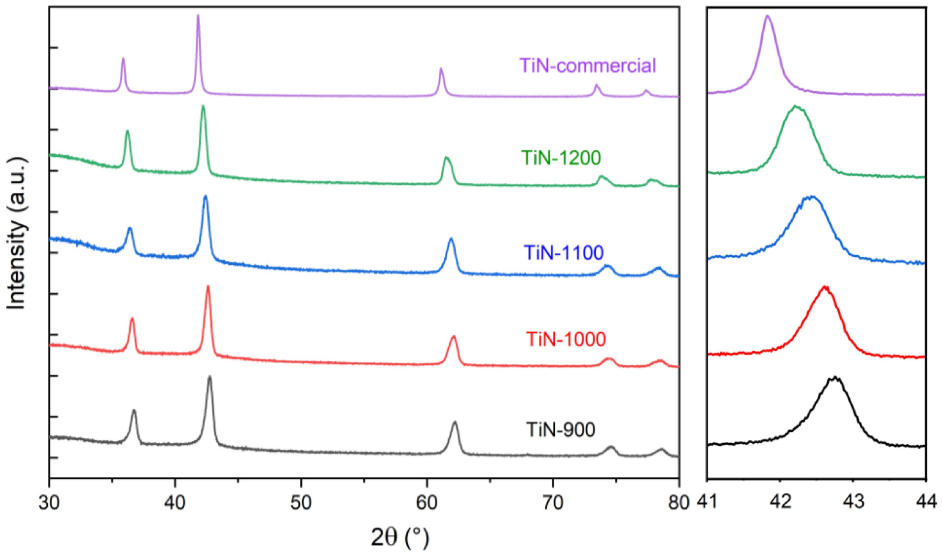


Figure 1. XRD patterns of TiN_xO_{1-x} samples produced by ammonolysis at different temperatures from 900 °C to 1200 °C (TiN-900 to TiN-1200) and a commercial TiN sample (TiN-commercial), where x was found to range from 0.53 to 1.0. A close up of the (200) peak is shown on the right.

© 2023 The Authors. ChemCatChem published by Wiley-VCH GmbH

18673899, 2023, 23, Downloaded from https://chemistry-europe.onlinelibrary.wiley.com/doi/10.1002/cctc.202300687 by Test, Wiley Online Library on [18/12/2023]. See the Terms and Conditions (https://onlinelibrary.wiley.com/terms-and-conditions) on Wiley Online Library for rules of use; OA articles are governed by the applicable Creative Commons License

surface composition, and indicate the presence of titanium dioxide, titanium oxynitride and titanium nitride (Figure 2 and Table S2). This can be attributed to the same exposure to air and humidity in these samples. The O 1s binding energy region showed three environments, one at ~529.5 eV that refers to metal-oxygen bonds,[31] one at ~531.8 eV that refers to metal nitrogen bonds,[32] and one at ~533 eV that refers to adventitious surface oxygen.[33] TiN-commercial exhibits a 100% bulk nitrogen occupancy, as determined by XRD analysis, whereas the surface is terminated by ~50% of oxides, as determined by XPS. The percentages of areas under the deconvoluted peaks of Ti 2p, N 1s and O 1s are presented in Figure 3 and Table S2. Surface TiO_2 seen at a binding energy of 458.5 eV,[34] accounts for 50–60% in Ti $2p_{3/2}$ spectra, with the fraction of TiN_xO_{1-x} remaining almost the same in the series of samples. In N 1s spectra, Ti–N components (397 eV)[35] are in majority (40–55%), corresponding to the presence of both TiN and TiN_xO_{1-x}, whereas N–O components (396 eV)[36] have a lower contribution (25–40%), corresponding to the presence of solely TiN_xO_{1-x}. The component of O–Ti in TiN-commercial from O 1s spectra holds the lowest fraction (~60%) compared with other oxynitrides (~70%), which agrees with what is seen in Ti 2p spectra. Therefore, it can be concluded that TiN-commercial has the highest TiN component both in the bulk and at the surface,

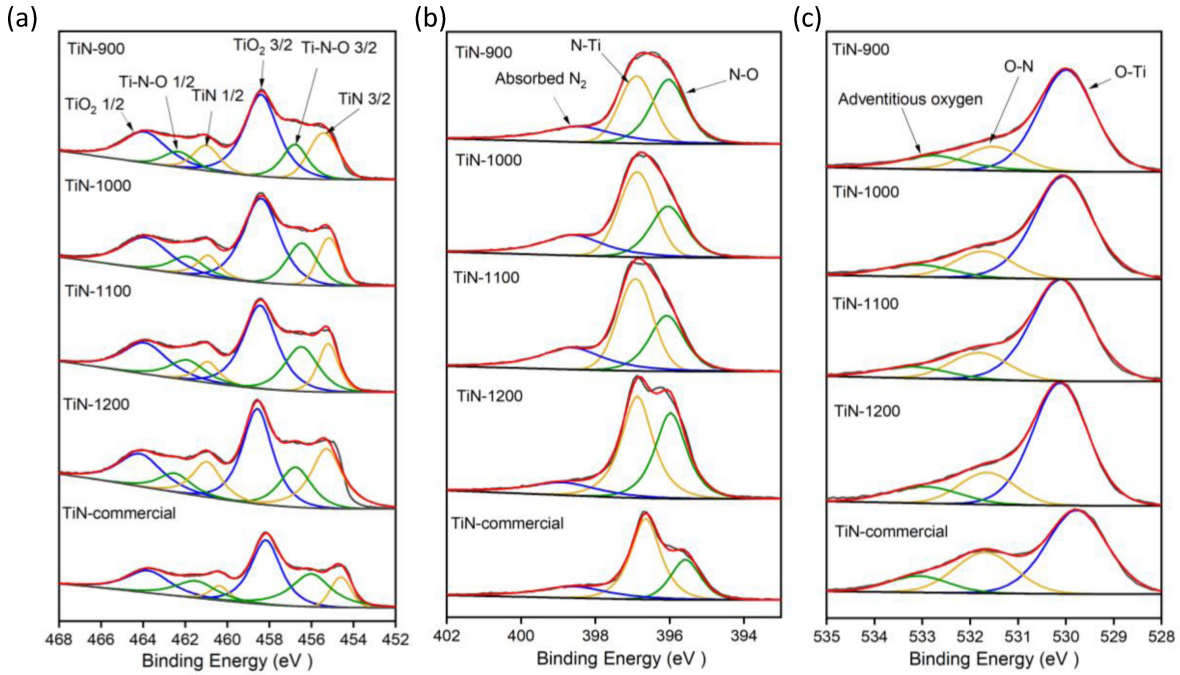


Figure 2. Close up of the XPS spectra of Ti 2p **(a)**, N 1s **(b)** and O 1s **(c)** binding energy regions in TiN_xO_{1-x} samples produced by ammonolysis at different temperatures from 900 °C to 1200 °C (TiN-900 to TiN-1200) and a commercial TiN sample (TiN-commercial). Peaks have been deconvoluted into their respective chemical environments.

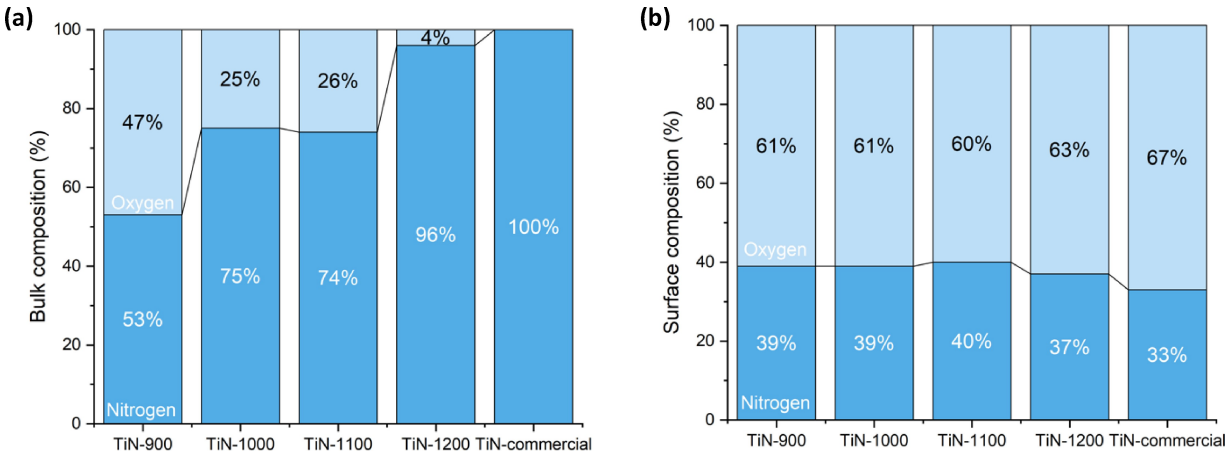


Figure 3. Bulk **(a)** and surface **(b)** composition ratio between oxygen and nitrogen in TiN_xO_{1-x} samples produced by ammonolysis at different temperatures from 900 °C to 1200 °C (TiN-900 to TiN-1200) and a commercial TiN sample (TiN-commercial). Bulk and surface compositions were derived from XRD modeling and XPS Ti-2p peaking fitting, respectively (Table S3).

© 2023 The Authors. ChemCatChem published by Wiley-VCH GmbH

18673899, 2023, 23, Downloaded from https://chemistry-europe.onlinelibrary.wiley.com/doi/10.1002/cctc.202300687 by Test, Wiley Online Library on [18/12/2023]. See the Terms and Conditions (https://onlinelibrary.wiley.com/terms-and-conditions) on Wiley Online Library for rules of use; OA articles are governed by the applicable Creative Commons License

whereas the as-synthesised oxynitrides have a similar nitrogen occupancy at the surface, but this varies significantly in the bulk.

Scanning electron microscope (SEM) images of all oxynitride samples and TiN-commercial were taken to study the surface morphologies and particle sizes. The morphology of the TiO_2 starting precursor was also measured for comparison. As can be seen in Figure 4, the higher annealing temperature under ammonia caused the TiO_2 precursor (around 100 nm wide, rounded particles) to agglomerate, and resulted in the formation of larger particles that showed a lower surface area (as measured by N_2 sorption at 77 K, discussed later).[37]

HER activities of all samples were measured by linear sweep voltammetry (Figure 5). The TiN-900 and TiN-1000 samples that possessed low nitrogen occupancy ($0.53 \leq x \leq 0.75$) exhibited similar activity, and showed a bump located between -0.40 to -0.50 V_{RHE}, which may be due to the reduction of oxynitride and removal of oxygen (Figure S3 and Figure S4). For the TiN-1100 and TiN-1200 oxynitride samples with higher nitrogen occupancy ($0.74 \leq x \leq 0.96$) and TiN-commercial standard, this bump was not observed, and the HER activities were seen to enhance with an increase in nitrogen occupancy. It is notable that the reduction of the oxynitride, found in samples TiN-900 and TiN-1000, will contribute to the overall current density (as TiN-1100 shows a perceived lower activity than TiN-1000). The earlier onset potentials of HER in TiN-1200 and TiN-commercial indicate that higher nitrogen occupancy is beneficial to HER activity.

To further investigate catalytic performance and eliminate the effect of surface area of catalysts, we normalised the geometric current density with ECSA and BET surface area (Table S4 and Figure 6). The BET surface area was determined *ex situ* through nitrogen adsorption/desorption tests, whereas ECSA was derived from the double layer capacitance. With regards to the BET surface area, higher annealing temperature results in a lower surface area. The lowest BET surface area was seen in TiN-commercial (9.82 m^2/g) and the highest BET surface area was seen in the least sintered sample TiN-900 (36.5 m^2/g). Topotactic growth was also observed in TiN-900, which usually happens during the formation of nitride and results in a higher surface area.[38]

The ECSA derived from non-Faradaic double layer capacitance (non-Faradaic region: 0.05 V_{RHE}–0.30 V_{RHE}, Figures S5 and S6) is plot against the BET surface area in Figure 7, and shows an approximately proportional relationship for TiN-1000, TiN-1100, TiN-1200 and TiN-commercial samples. However, this relationship was not seen in the TiN-900 and TiO_2 samples, where the highest BET surface areas and lowest ECSAs of all the samples were observed. This was attributed to the lower conductivity found in these samples and the resulting increase in dielectric behaviour. This means that the capacitance measured from the charging current is smaller than a double layer capacitance, which is often found in the more insulating

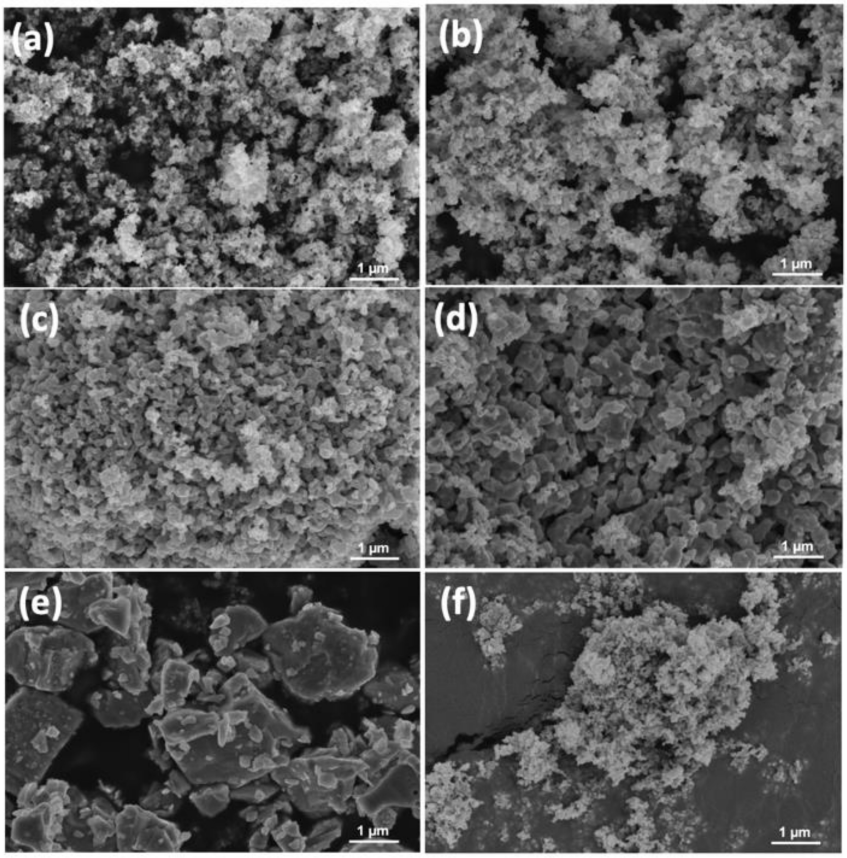


Figure 4. SEM images of (a) TiN-900, (b) TiN-1000, (c) TiN-1100, (d) TiN-1200, (e) TiN-commercial, and (f) the TiO_2 starting precursor.

© 2023 The Authors. ChemCatChem published by Wiley-VCH GmbH

18673899, 2023, 23, Downloaded from https://chemistry-europe.onlinelibrary.wiley.com/doi/10.1002/cctc.202300687 by Test, Wiley Online Library on [18/12/2023]. See the Terms and Conditions (https://onlinelibrary.wiley.com/terms-and-conditions) on Wiley Online Library for rules of use; OA articles are governed by the applicable Creative Commons License

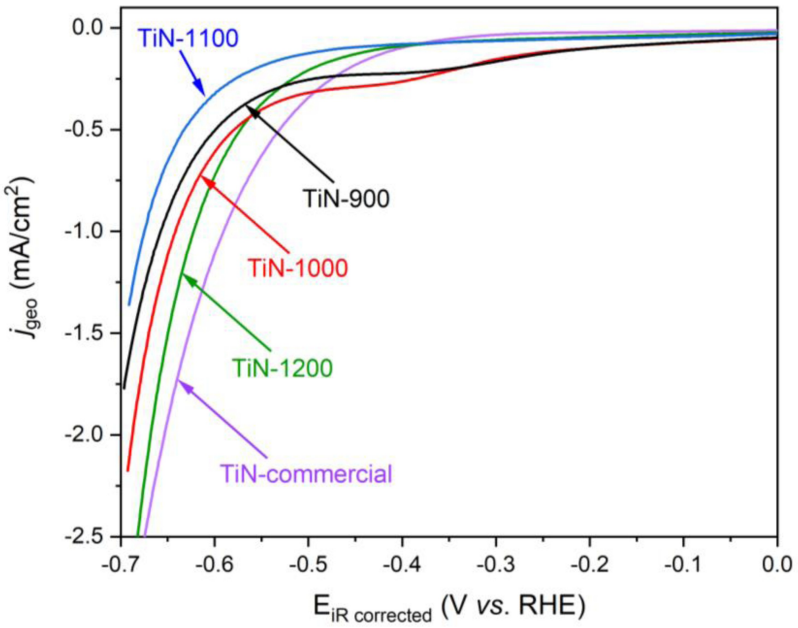


Figure 5. Geometric HER activities of TiN_xO_{1-x} samples produced by ammonolysis at different temperatures from 900 °C to 1200 °C (TiN-900 to TiN-1200) and a commercial TiN sample (TiN-commercial). Samples were measured in 0.5 M argon saturated $H_2SO_{4(aq)}$ at room temperature using an RDE setup. The results shown here are the third scan to the cathodic potentials. The rotation speed was 1600 rpm and the scan rate was 5 mV s^{-1}.

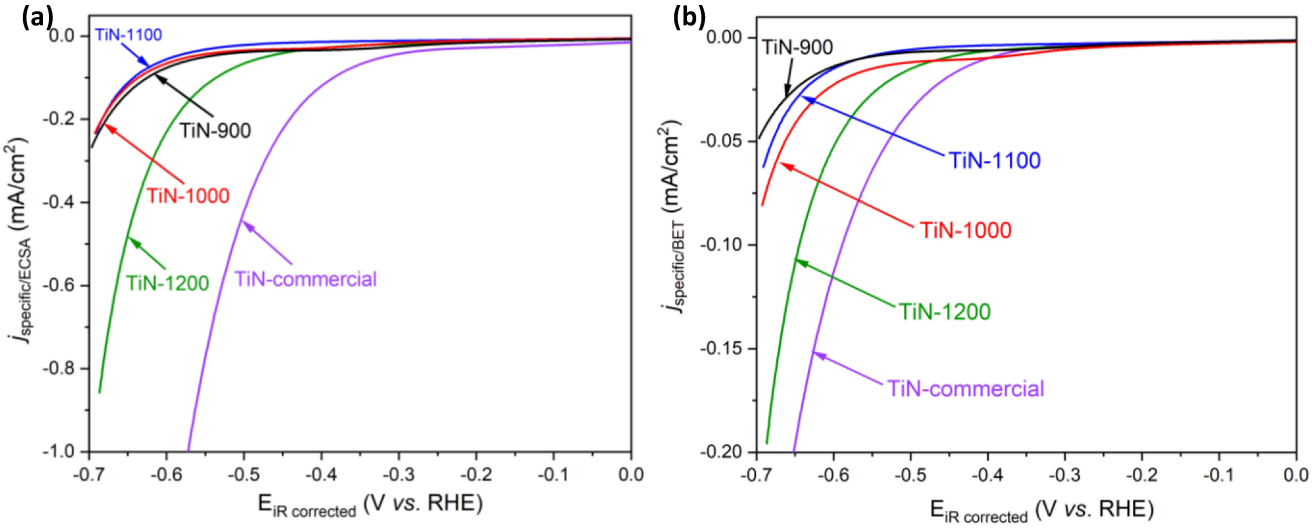


Figure 6. Specific HER activities normalised by (a) ECSA and (b) BET surface area of of TiN_xO_{1-x} samples produced by ammonolysis at different temperatures from 900 °C to 1200 °C (TiN-900 to TiN-1200) and a commercial TiN sample (TiN-commercial).

oxide catalysts.[39] However, the higher capacitance of the oxynitride (TiN-900) compared with the oxide (TiO_2) might be a result of proton ingress into the bulk,[40] which means that the oxynitrides tend to intercalate more protons than the oxide.

Although catalysts with higher surface area will generally possess higher electrochemical activity, our studies indicate that the nitrogen occupancy in the TiN lattice has a larger influence. Despite the lowest ECSA and BET surface, TiN-commercial exhibits the best geometric and specific activity owing to its high nitrogen occupancy ($x = 1.0$) and electrical conductivity (Figures 7 and 8). And thus, the HER activity of the oxynitride reduces as the bulk nitrogen occupancy decreases (and oxygen occupancy increases).

TiN-commercial was tested at a constant applied potential of $-0.6\ V_{RHE}$ in 0.5 M argon-saturated $H_2SO_{4(aq)}$ for 12 hours (Figure 9). A promoted current density was observed in the first 3 h of the test, which may indicate that a partial reduction of the material surface results in an increased activity (e.g. the surface oxidised layer is removed to produce a cleaner nitride surface). Furthermore, the high apparent stability of the TiN catalyst in highly acidic electrolyte (0.5 M $H_2SO_{4(aq)}$, pH~0) is demonstrated, with no significant loss in current density over the 12 h testing period. Nonetheless, we acknowledge that to

© 2023 The Authors. ChemCatChem published by Wiley-VCH GmbH

18673899, 2023, 23, Downloaded from https://chemistry-europe.onlinelibrary.wiley.com/doi/10.1002/cctc.202300687 by Test, Wiley Online Library on [18/12/2023]. See the Terms and Conditions (https://onlinelibrary.wiley.com/terms-and-conditions) on Wiley Online Library for rules of use; OA articles are governed by the applicable Creative Commons License

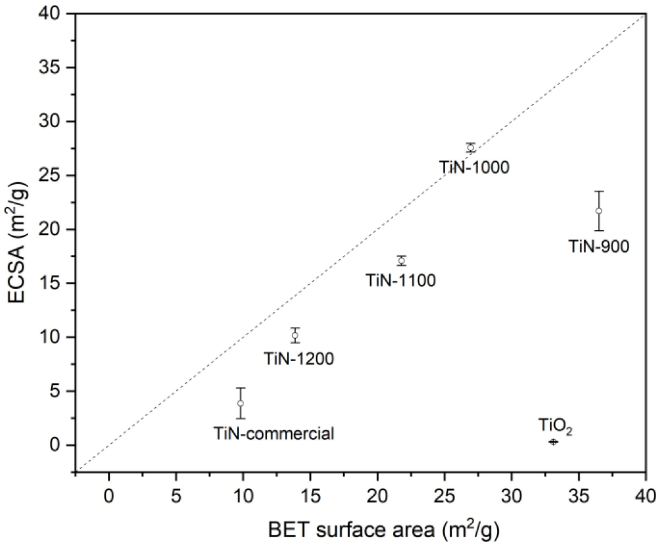


Figure 7. The comparison of the BET surface area and ECSA of TiN_xO_{1-x} samples produced by ammonolysis at different temperatures from 900 °C to 1200 °C (TiN-900 to TiN-1200) and a commercial TiN sample (TiN-commercial) and the starting precursor TiO_2. ECSA was determined by non-Faradaic double layer capacitance in non-Faradaic region (0.05 V_{RHE} to 0.3 V_{RHE}, Figure S5) with different scan rates of 160, 120, 100, 50, 20 mV/s in 0.5 M argon saturated 0.5 M $H_2SO_{4(aq)}$ at the rotation speed of 1600 rpm.

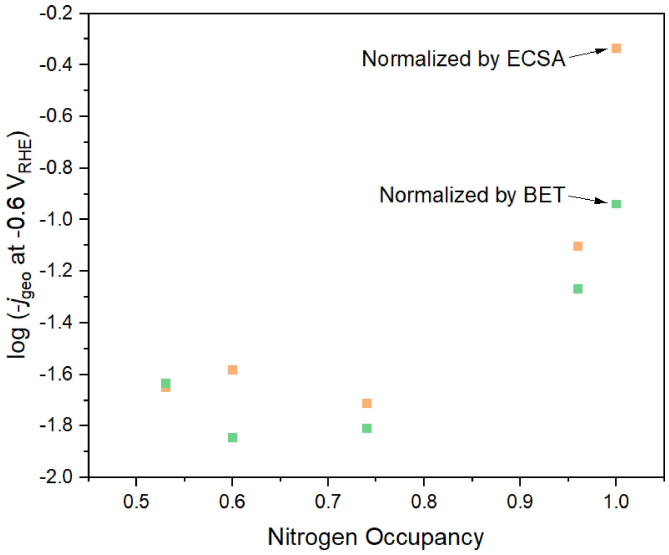


Figure 8. The logarithmic relationship seen between nitrogen occupancy and current density for the HER at −0.60 V_{RHE} for the TiN_xO_{1-x} samples produced by ammonolysis at different temperatures from 900 °C to 1200 °C (TiN-900 to TiN-1200) and a commercial TiN sample (TiN-commercial).

more definitely measure stability in such short term tests, complementary measures of dissolution rates are necessary, for instance by inductively coupled mass spectrometry (ICP-MS).[41–43]

For the stability tests carried out, it is understood that under the applied potentials and acidic conditions employed, any surface oxide species will be dissolved.[44] Our XPS studies showed that our TiON materials are indeed laden with surface oxides (Figure 2), which these nanoscale layers will likely

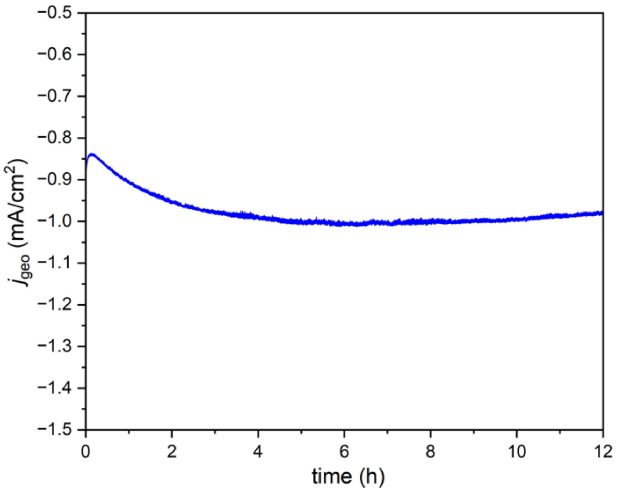


Figure 9. Chronoamperometry of the TiN-commercial sample driving the HER at −0.6 V_{RHE} for 12 hours in 0.5 M argon-saturated $H_2SO_{4(aq)}$ at the rotation speed of 1600 rpm.

dissolve under the conditions employed for our stability tests. Nevertheless, our materials showed high long-term stability. In fact, the electron flux over the analysis period was ~two orders of magnitude higher than the total Ti atoms available, which indicated that the dissolution process may have only occurred for the surface oxides present on our materials, or was a significantly slower process in comparison to the HER. We therefore postulate that dissolution of the native surface oxide layer in our oxynitrides results in the formation of a pure nitride surface that passivates the oxynitride bulk. This is evidenced by SEM images of an exemplar catalyst, TiN-commercial, carried out before and after a 12 h stability test, which showed no noticeable change in the structure of the material (Figure S8). Nevertheless, with regards to the oxynitrides produced in this study, it is possible that higher bulk oxygen content may result in more pronounced degradation under the HER conditions imposed.

Conclusions

In this work, we have tested the HER performance of a series of titanium oxynitrides (TiN_xO_{1-x}) and commercial TiN of cubic rock-salt structure with differing levels of bulk nitrogen occupancy. The TiN_xO_{1-x} were synthesised by annealing rutile TiO_2 nanopowders under ammonia at 900 °C–1200 °C, with a range of bulk nitrogen occupancy obtained ($0.53 \leq x \leq 0.96$). The commercial TiN showed no bulk oxygen occupancy ($x = 1.0$). Samples annealed at higher temperatures have a higher bulk nitrogen occupancy but possessed lower surface area (37 m^2/g at $x = 0.53$ *vs.* 10 m^2/g at $x = 1.0$), a larger crystallite size (15.43 nm at $x = 0.53$ *vs.* 72.94 nm at $x = 1.0$) and particle size (~100 nm at $x = 0.53$ *vs.* 2000 nm at $x = 1.0$). The surface areas were investigated by ECSA and BET methods. Our results demonstrate that oxygen incorporation into the nitride lattice is detrimental to the intrinsic conductivity and is the primary

© 2023 The Authors. ChemCatChem published by Wiley-VCH GmbH

18673899, 2023, 23, Downloaded from https://chemistry-europe.onlinelibrary.wiley.com/doi/10.1002/cctc.202300687 by Test, Wiley Online Library on [18/12/2023]. See the Terms and Conditions (https://onlinelibrary.wiley.com/terms-and-conditions) on Wiley Online Library for rules of use; OA articles are governed by the applicable Creative Commons License

cause of reduced specific HER activity, where the current density at $-0.6\ V_{RHE}$ reduced from $-0.115\ mA/cm^2$ at $x=1.0$ to $-0.0125\ mA/cm^2$ at $x=0.53$ (normalised by BET surface area) and from $-1.20\ mA/cm^2$ at $x=1.0$ to $-0.05\ mA/cm^2$ at $x=0.53$ (normalised by ECSA). Furthermore, all samples show an increased activity during prolonged (several hours) CA at $-0.6\ V_{RHE}$ (Figure S7), which we postulate is due the reduction and removal of surface oxide species at this reduced potential, resulting in a cleaner nitride surface. Future work is required to quantify the dissolution of titanium oxynitrides using ICP-MS.[45]

To conclude, even though the HER performance of the nitride materials produced herein is significantly lower than the commercial standard, Pt/C; the relatively high stability and conductivity of this material makes it a promising candidate for applications as a support (Table S5). This work has also suggested that minimising bulk oxygen content by annealing the precursor at higher temperatures will give a lower surface area and expose fewer active sites, which is a significant issue when using the nitride as a support material for electrocatalysts.

Experiments

Synthesis and characterisation of TiN_xO_{1-x}

Titanium(IV) dioxide (rutile, 99.5%, <100 nm particle size, Sigma-Aldrich) was used as the starting material for ammonolysis. Ammonia (99.98%) and argon (99.99(8)%) served as the reaction gas and the carrier gas, respectively.

Titanium dioxide (200 mg) was transferred to an alumina crucible. The crucible was placed inside a tube furnace and purged under argon and then ammonia at the rate of 250 cm^3/min for 15 min before heating. The furnace was then heated up at the rate of 10 °C/min under ammonia flow (150 cm^3/min) and held at the target temperature (900 °C, 1000 °C, 1100 °C and 1200 °C) for 3 hours. When the reaction was complete, the furnace was turned off and allowed to cool down naturally with the product inside under argon flow (50 cm^3/min) overnight. The products were denoted as TiN-900, TiN-1000, TiN-1100 and TiN-1200, where the numbers represent the maximum annealing temperature under ammonia flow. Commercially available TiN powder (<3 μm particle size, Sigma-Aldrich) was used as a reference, and is denoted TiN-commercial.

Physical characterisation

XRD patterns were measured using a modified Bruker AXS D2 diffractometer with parallel beam optics equipped with a LYNXEYE XE-T silicon strip detector. X-rays were generated from a Cu source ($V=30$ kV, $I=10$ mA) with Cu $K_{\alpha1}$ ($\lambda=1.54056$ Å) and $K_{\alpha2}$ ($\lambda=1.54439$ Å) emitted with an intensity ratio of 2:1. Patterns were collected within the angular range of 2θ between 5–85° with a step size of 0.02025° and scan speed of 1.0 s per step. The microstructures of the materials were investigated by the Scanning Electron Microscopy (SEM) using a Zeiss Auriga machine with an accelerating voltage of 5 kV. The chemical states of Ti, N and O were analysed by a Thermo Scientific K-Alpha + X-ray photoelectron spectrometer. Binding energies were adjusted to adventitious graphitic C (284.8 eV) and the deconvolution was conducted using CasaXPS. Nitrogen isothermal adsorption/desorption was conducted on a Micromeritics Tristar II Plus at 77 K. The BET equation was used to estimate the total surface area, where the fitting region was determined by the Rouquerol method.[46] Before measurements, samples were degassed at 200 °C for 16 h under vacuum. Gases used were nitrogen (N5.2 CP grade) for adsorption/desorption and He (N5.0 CP grade) for the free-space measurement.

Electrochemical characterisation

To prepare the working electrode, 1.0 mL of a mixture of Millipore water (18.2 MΩ) and IPA with the volume ratio of 20:80 was added to 9.80 mg (± 0.10 mg) of the catalyst powder to form an ink. The ink suspension was then sonicated (RS Ultrasonic cleaner, 100 W) for 10 min in ice water. 10 μL of Nafion (5 wt.%, Merck) was added to the ink and the solution was sonicated for another 20 min. A 5 mm-diameter glassy carbon disk (SIGRADUR G, 0.196 cm^2) polished to a mirror-like surface with a silica suspension and a polishing pad was used as the working electrode, mounted into a Pine instrument Company E6-series ChangeDisk RDE assembly and affixed to a WaveVortex electrode rotator. Prior to drop casting, the GC disk was sonicated sequentially in ultrapure water and 2-propanol, each for 10 min. The ink was drop cast onto the working electrode right after sonication. 10 μL of the catalyst ink was drop cast to give a catalyst mass loading of 0.50 mg cm^{-2}. Electrochemical measurements were carried out in a jacketed three-electrode glass cell with a reference electrode (a reversible hydrogen electrode (RHE) immersed in an electrolyte filled Luggin capillary) and a counter electrode (carbon rod), as well as a gas inlet. The electrolyte was purged under argon for 10 min prior to each test to displace any oxygen dissolved in the electrolyte. The HER activities of as-synthesised catalysts were recorded using a Biologic SP-300 potentiostat and EC-Lab software with the rotation speed of 1600 rpm at room temperature. The three-electrode cell was filled with fresh electrolyte, 0.5 M H_2SO_4 (diluted from Merck Suprapur 96%, 99.999% trace metal basis H_2SO_4 stock), before each set of tests. The geometric activities were measured using linear sweep voltammetry (LSV), which was carried out at a rate of 5 mV/s from 0.1 to $-0.7\ V_{RHE}$. Each sample was scanned for three times and the third scan was plotted for comparison.

The specific current density was obtained by normalising geometric current density with electrochemically active surface area (ECSA) and BET surface area. Electrochemical impedance spectroscopy (EIS) was carried out over the range of 200 kHz to 100 mHz under a DC potential of $-0.6\ V_{RHE}$ with the sinus amplitude of 10 mV (Figure S1). Initial stability tests were attained by using chronoamperometry (CA) by measuring the current density when holding the potential at $-0.6\ V_{RHE}$ for 10 h in an argon atmosphere. All data were corrected for ohmic losses via Equation 1 manually, where E_0 is the measured data, E is the corrected data and i is the current. Uncompensated resistance (R_u) was derived by high-frequency intercept fitting of the Nyquist plot.

$$E = E_0 - iR_u \quad (1)$$

Acknowledgements

G. Y. thanks Imperial College London for the President's PhD Scholarship. M. W. thanks the EPSRC Centre for Doctoral Training in the Advanced Characterisation of Materials (grant number EP/L015277/1). A. K. thanks the EPSRC Catalytics plasmonics programme EP/W017075/1. The authors thank Prof. Camille Petit and Prof. Stephen Skinner for the help with the ammonolysis process.

© 2023 The Authors. ChemCatChem published by Wiley-VCH GmbH

18673899, 2023, 23, Downloaded from https://chemistry-europe.onlinelibrary.wiley.com/doi/10.1002/cctc.202300687 by Test, Wiley Online Library on [18/12/2023]. See the Terms and Conditions (https://onlinelibrary.wiley.com/terms-and-conditions) on Wiley Online Library for rules of use; OA articles are governed by the applicable Creative Commons License

Conflict of Interests

The authors declare no conflict of interest.

Data Availability Statement

The data that support the findings of this study are available from the corresponding author upon reasonable request.

Keywords: Ammonolysis · hydrogen evolution reaction · nitrogen occupancy · PEM electrolysers · titanium oxynitrides

[1] W. S. Broecker, *Science* **1975**, *189*, 460–463.
[2] N. Gruber, *Philos. Trans. R. Soc. London* **2011**, *369*, 1980–1996.
[3] L. Bertuccioli, A. Chan, D. Hart, B. Madden, Development of Water Electrolysis in the European Union. *Fuel cells and hydrogen joint undertaking*, **2014**.
[4] P. C. K. Vesborg, T. F. Jaramillo, *RSC Adv.* **2012**, *2*, 7933–7947.
[5] N. Han, P. Liu, J. Jiang, L. Ai, Z. Shao, S. Liu, *J. Mater. Chem. A* **2018**, *6*, 19912–19933.
[6] Y. Han, X. Yue, Y. Jin, X. Huang, P. K. Shen, *J. Mater. Chem. A* **2016**, *4*, 3673–3677.
[7] Y. Liu, T. Sakthivel, F. Hu, Y. Tian, D. Wu, E. H. Ang, H. Liu, S. Guo, S. Peng, Z. Dai, *Adv. Energy Mater.* **2023**, *13*, 2203797.
[8] B. Avasarala, P. Haldar, *Electrochim. Acta* **2010**, *55*, 9024–9034.
[9] D. Yuan, Y. Jiao, Z. Li, X. Chen, J. Ding, W. L. Dai, H. Wan, G. Guan, *Adv. Mater. Interfaces* **2021**, *8*, 1–8.
[10] R. Jamil, R. Ali, S. Loomba, J. Xian, M. Yousaf, K. Khan, B. Shabbir, C. F. McConville, A. Mahmood, N. Mahmood, *Chem Catal.* **2021**, *1*, 802–854.
[11] X. Peng, C. Pi, X. Zhang, S. Li, K. Huo, P. K. Chu, *Sustain. Energy Fuels* **2019**, *3*, 366–381.
[12] A. Valour, M. A. U. Higuita, G. Guillonneau, N. Crespo-Monteiro, D. Jamon, M. Hochedel, J. Y. Michalon, S. Reynaud, F. Vocanson, C. Jiménez, M. Langlet, C. Donnet, Y. Jourlin, *Surf. Coat. Technol.* **2021**, *413*, 127089.
[13] A. Bakri, M. Sahdan, F. Adriyanto, N. Raship, N. D. Said, S. Abdullah, M. Rahim, in *AIP Conference Proceedings 1788*, **2017**, p. 030030.
[14] E. Pastor, M. Sachs, S. Selim, J. R. Durrant, A. A. Bakulin, A. Walsh, *Nat. Rev. Mater.* **2022**, *7*, 503–521.
[15] Q. Luo, C. Lu, L. Liu, M. Zhu, *Green Energy and Environment* **2023**, *8*, 406–437. DOI: 10.1016/j.gee.2022.07.002.
[16] A. Fujishima, X. Zhang, D. A. Tryk, *Surf. Sci. Rep.* **2008**, *63*, 515–582.
[17] R. Asahi, T. Morikawa, T. Ohwaki, K. Aoki, Y. Taga, *Science* **2001**, *293*, 269–271.
[18] J. B. Yoo, H. J. Yoo, H. J. Jung, H. S. Kim, S. Bang, J. Choi, H. Suh, J. H. Lee, J. G. Kim, N. H. Hur, *J. Mater. Chem. A* **2016**, *4*, 869–876.
[19] H. Von Seefeld, N. W. Cheung, M. Mäenpää, M. A. Nicolet, *IEEE Trans. Electron Devices* **1980**, *27*, 873–876.
[20] Y. Han, X. Yue, Y. Jin, X. Huang, P. K. Shen, *J. Mater. Chem. A* **2016**, *4*, 3673–3677.
[21] J. Zhang, A. Reda, X. Zhao, X. Peng, Y. Song, H. Xia, *Appl. Surf. Sci.* **2022**, *598*, 153745.
[22] J. Zhao, Y. Zeng, J. Wang, Q. Xu, R. Chen, H. Ni, G. J. Cheng, *Nanoscale* **2020**, *12*, 15393–15401.
[23] E. Furimsky, *Appl. Catal. A* **2003**, *240*, 1–28.
[24] M. E. Kreider, M. B. Stevens, Y. Liu, A. M. Patel, M. J. Statt, B. M. Gibbons, A. Gallo, M. Ben-Naim, A. Mehta, R. C. Davis, A. V. Ievlev, J. K. Nørskov, R. Sinclair, L. A. King, T. F. Jaramillo, *Chem. Mater.* **2020**, *32(7)*, 2946–2960. DOI: 10.1021/acs.chemmater.9b05212.
[25] N. R. Mucha, J. Som, J. Choi, S. Shaji, R. K. Gupta, H. M. Meyer, C. L. Cramer, A. M. Elliott, D. Kumar, *ACS Appl. Energ. Mater.* **2020**, *3*, 8366–8374.
[26] K. Kamiya, T. Yoko, M. Bessho, *J. Mater. Sci.* **1987**, *22*, 937–941.
[27] J. Graciani, S. Hamad, J. F. Sanz, *Phys. Rev. B: Condens. Matter Mater. Phys.* **2009**, *80*, 1–10.
[28] L. Vegard, *Zeitschrift für Krist. - Cryst. Mater.* **1928**, *67*, 239–259.
[29] N. C. Saha, H. G. Tompkins, *J. Appl. Phys.* **1992**, *72*, 3072–3079.
[30] A. Lippitz, T. Hübert, *Surf. Coat. Technol.* **2005**, *200*, 250–253.
[31] A. M. Alotaibi, P. Promdet, G. B. Hwang, J. Li, S. P. Nair, S. Sathasivam, A. Kafizas, C. J. Carmalt, I. P. Parkin, *ACS Appl. Mater. Interfaces* **2021**, *13*, 10480–10489.
[32] Y. Liu, Y. Wang, Y. Zhang, Z. You, X. Lv, *J. Am. Ceram. Soc.* **2020**, *103*, 3905–3916.
[33] H. Liu, Y. Zhao, Y. Liu, T. Liang, Y. Tian, T. Sakthivel, S. Peng, S. Y. Kim, Z. Dai, *Chem. Commun.* **2023**, *59*, 2931–2934.
[34] A. Glaser, S. Surnev, F. P. Netzer, N. Fateh, G. A. Fontalvo, C. Mitterer, *Surf. Sci.* **2007**, *601*, 1153–1159.
[35] N. Sun, J. Xu, D. Zhou, P. Zhao, S. Li, J. Wang, S. Chu, F. Ali, *J. Mater. Sci. Mater. Electron.* **2018**, *29*, 10170–10176.
[36] N. Sun, D. Zhou, W. Liu, S. Shi, Z. Tian, F. Liu, S. Li, J. Wang, F. Ali, *ACS Sustainable Chem. Eng.* **2020**, *8*, 7869–7878.
[37] C. Gebauer, P. Fischer, M. Wassner, T. Diemant, Z. Jusys, N. Hüsing, R. J. Behm, *Nano Energy* **2016**, *29*, 136–148.
[38] L. Volpe, M. Boudart, *J. Solid State Chem.* **1985**, *59*, 332–347.
[39] S. Jung, C. C. L. McCrory, I. M. Ferrer, J. C. Peters, T. F. Jaramillo, *J. Mater. Chem. A* **2016**, *4*, 3068–3076.
[40] J. H. L. Hadden, M. P. Ryan, D. J. Riley, *ACS Appl. Energ. Mater.* **2020**, *3*, 2803–2810.
[41] S. Cherevko, S. Geiger, O. Kasian, N. Kulyk, J. Grote, A. Savan, B. Ratna, S. Merzlikin, B. Breitbach, A. Ludwig, K. J. J. Mayrhofer, *Catal. Today* **2016**, *262*, 170–180.
[42] R. Frydendal, E. A. Paoli, B. P. Knudsen, B. Wickman, P. Malacrida, I. E. L. Stephens, I. Chorkendorff, *ChemElectroChem* **2014**, *1*, 2075–2081.
[43] A. A. Topalov, I. Katsounaros, M. Auinger, S. Cherevko, J. C. Meier, S. O. Klemm, K. J. J. Mayrhofer, *Angew. Chem. Int. Ed.* **2012**, *51*, 12613–12615.
[44] M. J. Muñoz-Portero, J. García-Antón, J. L. Guiñón, L. Leiva-García, *Corros. Sci.* **2011**, *53*, 1440–1450.
[45] M. Ledendecker, J. S. Mondschein, O. Kasian, S. Geiger, D. Gçhl, M. Schalenbach, A. Zeradjanin, S. Cherevko, R. E. Schaak, K. Mayrhofer, *Angew. Chem. Int. Ed.* **2017**, *56*, 9767–9771.
[46] J. Rouquerol, F. Rouquerol, P. Llewellyn, G. Maurin, K. S. W. Sing, *Adsorpt. by Powders Porous Solids Princ. Methodol. Appl. Second Ed.* **2013**, 220–223.
[47] B. H. Toby, *J. Appl. Crystallogr.* **2001**, *34*, 210–213.
[48] C. P. Kempter, *Phys. Status Solidi* **1966**, *18*, K117–K118.
[49] Y. Djaoued, R. Taj, R. Brüning, S. Badilescu, P. V. Ashrit, G. Bader, T. Vo-Van, *J. Non-Cryst. Solids* **2002**, *297*, 55–66.
[50] C. C. L. McCrory, S. Jung, I. M. Ferrer, S. M. Chatman, J. C. Peters, T. F. Jaramillo, *J. Am. Chem. Soc.* **2015**, *137*, 4347–4357.
[51] C. C. L. McCrory, S. Jung, J. C. Peters, T. F. Jaramillo, *J. Am. Chem. Soc.* **2013**, *135*, 16977–16987.
[52] A. Norlin, J. Pan, C. Leygraf, *J. Electrochem. Soc.* **2005**, *152*, J7.
[53] M. Smiljanic, S. Panic, M. Bele, F. Ruiz-zepeda, L. Pavko, L. Gas, A. Kokalj, M. Gabers, N. Hodnik, *ACS Catal.* **2022**, *12*, 13021–13033.
[54] Y. Yang, D. Wu, R. Li, P. Rao, J. Li, P. Deng, J. Luo, W. Huang, Q. Chen, Z. Kang, Y. Shen, X. Tian, *Appl. Catal. B* **2022**, *317*, 121796.
[55] C. Wang, H. Shi, H. Liu, J. Fu, D. Wei, W. Zeng, Q. Wan, G. Zhang, H. Duan, *Electrochim. Acta* **2018**, *292*, 727–735.
[56] S. Yang, J. Kim, Y. J. Tak, A. Soon, H. Lee, *Angew. Chem. Int. Ed.* **2016**, *55*, 2058–2062.
[57] S. Tang, B. Ouyang, H. Tan, W. Zhou, Z. Ma, Y. Zhang, *Electrochim. Acta* **2020**, *362*, 137222.

Manuscript received: May 26, 2023
Revised manuscript received: September 20, 2023
Accepted manuscript online: September 27, 2023
Version of record online: November 22, 2023

© 2023 The Authors. ChemCatChem published by Wiley-VCH GmbH

18673899, 2023, 23, Downloaded from https://chemistry-europe.onlinelibrary.wiley.com/doi/10.1002/cctc.202300687 by Test, Wiley Online Library on [18/12/2023]. See the Terms and Conditions (https://onlinelibrary.wiley.com/terms-and-conditions) on Wiley Online Library for rules of use; OA articles are governed by the applicable Creative Commons License